Nanoscale

PAPER

View Article Online
View Journal | View Issue

Cite this: *Nanoscale*, 2020, **12**, 13582

Preclinical evaluation of platinum-loaded hydroxyapatite nanoparticles in an embryonic zebrafish xenograft model†

Robin A. Nadar, ‡[a] Nandini Asokan, ‡[b,c] Lorenzo Degli Esposti, [d] Alessandra Curci, [e] Alessandra Barbanente, [e] Lukas Schlatt,[f] Uwe Karst, [f] Michele Iafisco, [d] Nicola Margiotta, [e] Michael Brand, [b] Jeroen J. J. P. van den Beucken, [a] Martin Bornhäuser [b,c,g,h] and Sander C. G. Leeuwenburgh *[a,d]

Hydroxyapatite (HA) nanoparticles are commonly used as building blocks in the design of bone-substituting biomaterials. Recently, these nanoparticles have been considered for the treatment of metastasis disease, since their pH-dependent dissolution behavior allows for precise tuning of release kinetics of loaded cargo. Herein we show that the capacity of drug-loaded nanoparticles stabilized with citrate ions reduce cancer cell survival in an embryonic zebrafish xenograft model. In particular, *in vitro* studies demonstrate that PtPP-loaded HA nanoparticles exhibit anti–proliferative activity against breast cancer cells at reduced pH. *In vivo* studies using an embryonic zebrafish xenograft model reveal that PtPP co-delivered with human breast cancer cells strongly reduce cancer cell survival. Similarly, co-injection of breast cancer cells with citrate-functionalized and PtPP-loaded HA nanoparticles into zebrafish significantly reduces survival of cancer cells due to release of chemotherapeutically active kiteplatin species. These results demonstrate the preclinical efficacy of drug-loaded nanoparticles against human breast cancer cells in a xenogenic embryonic *in vivo* model.

Received 27th May 2020,
Accepted 10th June 2020

DOI: 10.1039/d0nr04064a

rsc.li/nanoscale

Introduction

Bone is a dynamic structure with the ability to heal after a fracture, trauma or disease. When this self-healing capacity is not sufficient, suitable bone grafts can be used to stimulate the healing response of the human body.[1] Nevertheless, bone diseases or disorders often require additional delivery of drugs at the injury or fracture site to combat these degenerative diseases effectively. Unfortunately, several bone diseases such as osteoporosis, bone cancer, and secondary metastases in bone cannot be treated effectively.[2] Unlike traditional oral and intravenous systems for systemic drug delivery, local delivery systems enable efficient delivery of chemotherapeutic agents at high concentrations within the affected sites. Consequently, therapeutic efficacy can be maximized and adverse systemic side effects minimized. Among the various types of nanocarriers, nanosized bioceramics such as calcium phosphate (CaP) nanoparticles are particularly attractive for treatment of bone cancer in view of their excellent biocompatibility, bioactivity, stability, and pH-dependent dissolution characteristics.[3]

CaPs are currently used as synthetic bone substitute materials since their composition resembles the mineral phase of bone. This mineral phase of the extracellular bone

[a]*Department of Dentistry - Regenerative Biomaterials, Radboud Institute for Molecular Life Sciences, Radboud University Medical Center, Philips van Leydenlaan 25, 6525 EX Nijmegen, the Netherlands.*
E-mail: sander.leeuwenburgh@radboudumc.nl
[b]*Center for Regenerative Therapies Dresden (CRTD), Technische Universität Dresden, Fetscherstrasse 105, 01307 Dresden, Germany*
[c]*Division of Hematology, Oncology and Stem Cell Transplantation, Department of Medicine I, University Hospital Carl Gustav Carus, Technische Universität Dresden, Fetscherstrasse 74, 01307 Dresden, Germany*
[d]*Institute of Science and Technology for Ceramics (ISTEC), National Research Council (CNR), Via Granarolo 64, 48018 Faenza, Italy*
[e]*Dipartimento di Chimica, Università degli Studi di Bari Aldo Moro, Via E. Orabona 4, 70125 Bari, Italy*
[f]*Institute of Inorganic and Analytical Chemistry, University of Münster, Corrensstraße 30, 48149 Münster, Germany*
[g]*National Center for Tumor Diseases (NCT), Fetscherstrasse 74/PF 64, 01307 Dresden, Germany*
[h]*German Consortium for Translational Cancer Research (DKTK), DKFZ, D-69120 Heidelberg, Germany*

†Electronic supplementary information (ESI) available. See DOI: 10.1039/d0nr04064a

‡These authors contributed equally to this work.

matrix consists of platelet-like hydroxyapatite (HA) crystals of few nanometers in thickness and several tens of nanometers in length.[4] Moreover, HA is well known for its capability to bind to a wide variety of molecules and therapeutic agents, which is attributed to its surface-reactive hydrated layer[5] and the presence of available surface ionic sites such as calcium cations and phosphate anions.[6] Additionally, when compared to other inorganic nanocarriers for drug delivery (*e.g.* silica, quantum dots, carbon nanotubes, and magnetic particles), HA nanoparticles exhibit excellent biocompatibility and low toxicity, while these particles can be produced and stored in a facile manner at low cost.[3,7]

Platinum (Pt)-based chemotherapeutics such as cisplatin are commonly used for treatment of bone cancer since these compounds induce cancer cell apoptosis by binding to DNA and forming Pt–DNA adducts.[8,9] Recently, HA nanoparticles have been reported as suitable nanocarriers for local delivery of novel Pt compounds functionalized with HA-binding bisphosphonate or pyrophosphate ligands.[10–15] These HA-binding ligands influenced both the loading of platinum onto and subsequent release from HA nanocrystals.[11,12] These findings suggest that HA nanoparticles retain these bisphosphonate or pyrophosphates ligands at their surface and release chemotherapeutically active derivatives of the Pt compounds. As such, Pt-loaded HA nanocarriers potentially not only can deliver their cargo at the tumor sites in a controlled manner, but also may improve the cytotoxicity of the unmodified complexes; consequently, they can be considered as platinum prodrugs.[13,14]

Here, we explore the feasibility of local release of kiteplatin, [$PtCl_2$(*cis*-1,4-DACH)] (DACH = diaminocyclohexane), or its solvato-species from HA nanoparticles. Kiteplatin is known for its robust anticancer activity against cisplatin- and oxaliplatin-resistant cell lines owing to the formation of more effective adducts with target DNA.[16,17] Recently, Curci *et al.* reported novel kiteplatin-pyrophosphate compounds (*i.e.* [Pt(dihydrogenpyrophosphate)(*cis*-1,4-DACH)], PtPP; Fig. 1A), which are stable at physiological pH, but rapidly hydrolyze at acidic pH releasing chemotherapeutically active kiteplatin species.[18] In addition, PtPP were activated intracellularly, producing kiteplatin species capable of platination of DNA upon substitution of the pyrophosphate ligand.[19] Thus, here we sought to asses if PtPP-loaded HA nanoparticles can be used as a smart pH-responsive delivery vehicle exerting strong inhibitory effects against cancer cells at a very low therapeutic dose *in vivo*.

To confirm the therapeutic efficacy of PtPP-loaded HA nanoparticles, various models can be used for screening of potential anticancer drugs. Conventionally, immunocompromised murine models have been used to understand the biology of metastasis, identify the role of oncogenes, and study the effects of chemotherapeutic drugs *in vivo*.[20] Nevertheless, several drawbacks are associated with the use of these models including the long duration for engraftment of tumor cells, the high amounts of cancer cells and drugs required, and the incompatibility with high-throughput drug screening.[21] In view of this, zebrafish models have been advocated recently as an alternative model to study tumor development, tumor progression, metastasis, and drug screening.[22–31] Zebrafish embryos are also increasingly used to explore the toxic and phenotypic effects of nanoparticles for their application in biomedicine.[32–34] However, zebrafish embryos have not been used for direct evaluation of the therapeutic efficacy of drug-loaded HA nanoparticles. Therefore, here we used for the first time an embryonic zebrafish xenograft model to investigate the application of PtPP-loaded HA nanoparticles to deliver active kiteplatin species *in vivo*.

Herein, we select human breast cancer cells (MDA-MB-231_eGFP) to investigate the anticancer activity of PtPP-loaded HA nanoparticles, since bone metastases frequently originate from primary breast tumors. The colloidal stability of platelet-shaped HA nanoparticles was improved using sodium citrate (Cit) as an effective dispersant.[35] The release kinetics of Pt from PtPP-loaded HA nanoparticles were shown to depend on pH, while the anticancer activity of these releases against cultured breast cancer cells was confirmed *in vitro*. Co-injection of free PtPP with breast cancer cells into embryonic zebrafish reduced the number of cancer cells at 2 days post injection (dpi) *in vivo*. Finally, we confirm the capacity of PtPP-loaded HA nanoparticles to decrease tumor cells *in vivo*, as evidenced by reduction of cancer cell survival in embryonic zebrafish in a manner comparable to systemic delivery of PtPP.

Results

Synthesis and characterization of PtPP-loaded HA nanoparticles

Platelet-shaped HA nanoparticles were synthesized according to established procedures.[13,36] HA nanoparticles were characterized by means of X-ray Diffraction (XRD) and Fourier-Transform Infrared Spectroscopy (FTIR) (Fig. S1†) which confirmed that they are composed of HA pure phase. Adsorption of citrate ions onto HA nanoparticles endows them with a strongly negative surface charge, thereby enhancing the colloidal stability of HA nanoparticles (Fig. S2†). The stability of citrate-functionalized HA nanoparticles remained almost similar over a period of 8 weeks (Table S1†). Transmission electron microscopy (TEM) images confirmed the presence of clustered platelet-shaped HA (Fig. 1B) as compared to dispersed platelet-like HA nanoparticles upon adsorption of citrate (HA-Cit) (Fig. 1C).

[Pt(dihydrogenpyrophosphate)(*cis*-1,4-DACH)] (PtPP) was synthesized as reported previously.[18] We investigated the influence of citrate addition on drug loading efficiency in more detail by adsorbing (i) citrate first (CF), (ii) drug first (DF), or (iii) simultaneous addition of citrate and drug (S). Further, the effect of PtPP loading on the physicochemical properties of HA nanoparticles was studied by measuring their particle size, polydispersity index and zeta potential (Fig. S2† and Table S2†) using Dynamic Light Scattering (DLS) and laser doppler electrophoresis. Adsorption of the drug prior to citrate

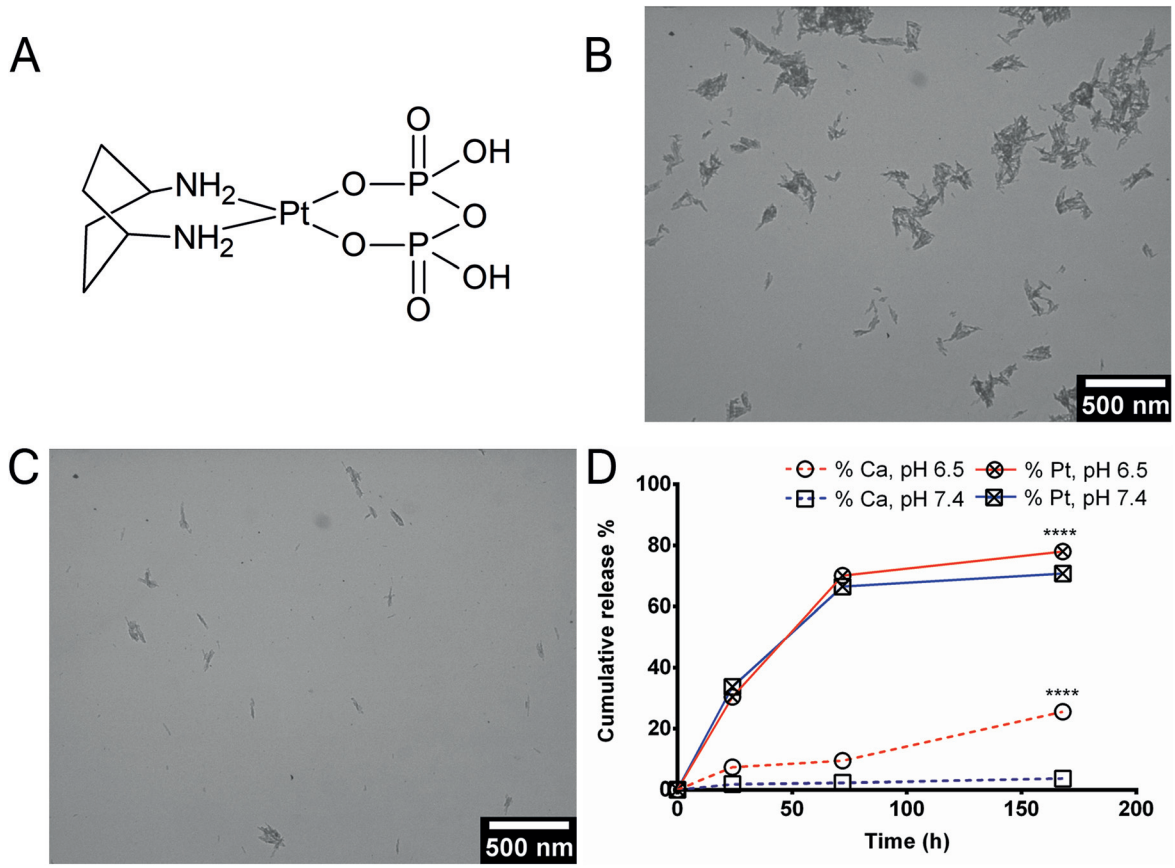

Fig. 1 Characterization of PtPP-loaded HA nanoparticles. (A) Chemical structure of [Pt(dihydrogenpyrophosphate)(*cis*-1,4-DACH)] (PtPP). TEM images of synthesized HA nanoparticles with (B) platelet-shaped morphology and (C) HA nanoparticles stabilized using citrate as dispersant (scale bar = 500 nm). (D) Cumulative release (%) of Platinum (Pt) and Calcium (Ca) from PtPP-loaded HA nanoparticles at pH 6.5 and 7.4. ****$P < 0.0001$.

resulted in a colloidally stable system with a particle size of 183 nm and the highest drug loading efficiency (8.9 ± 0.7 wt%). Consequently, PtPP was adsorbed prior to citrate in further experiments.

Acidic pH accelerates Pt and Ca release from HA nanoparticles

Pt and Ca release from HA nanoparticles functionalized with citrate ions and loaded with PtPP was monitored over a period of 7 days at 37 °C for different pH values (6.5 and 7.4; Fig. 1D and Table S3†). The lower pH value (6.5) was selected to mimic the acidic cancer microenvironment.[37,38] Pt release was not accelerated under acidic conditions at 24 h, but after 72 h more Pt was released from the HA nanoparticles at acidic *vs.* neutral conditions. The calcium release profile clearly demonstrated that more calcium was released at 24, 72 and 168 h under acidic *vs.* neutral conditions, which was attributed to the higher solubility of HA nanoparticles at lower pH. However, the difference in Pt or Ca release at varying pH is only statistically significant at 72 h.

PtPP is cytotoxic for human breast cancer cells *in vitro*

Potential cytotoxic effects of Pt drugs were evaluated with human breast (MDA-MB-231_eGFP) cancer cells, which are known to metastasize to bone.[39] The CCK-8 assay was used to determine the effects of Pt drugs on cell viability (after 72 h of exposure time). The anti-proliferative activity of Pt drugs was measured by quantifying DNA content after performing the CCK-8 assay. Half maximal inhibitory concentrations (IC_{50}), calculated from the dose-survival curves, are shown in Fig. 2A–D.

Fig. 2A shows that breast cancer cells viability was reduced most efficiently by kiteplatin (IC_{50} of 18.9 μM) followed by cisplatin (IC_{50} of 28.1 μM) and PtPP (IC_{50} of 73.7 μM). Based on the proliferation assay, cisplatin (IC_{50} = 13.1 μM) and kiteplatin (IC_{50} = 12.1 μM) exhibited comparable IC_{50} values for breast cancer cells, whereas PtPP (IC_{50} = 36.3 μM) were less cytotoxic (Fig. 2B). Contrarily, PtPP reduced the viability of the cancer cells more effectively at reduced pH. Fig. 2C shows that the IC_{50} of PtPP reduced by a factor of ~2 by decreasing the pH from 7.4 to 5.5. Based on the proliferation assay, exposure of PtPP to acidic conditions decreased the IC_{50} values by a factor of ~2 and ~4 (relative to neutral pH) at pH values of 6.5 and 5.5, respectively (Fig. 2D).

PtPP-loaded HA nanoparticles reduce proliferation of human breast cancer cells by releasing Pt *in vitro*

The viability and proliferation of breast cancer cells exposed to Pt species released from PtPP-loaded HA nanoparticles was

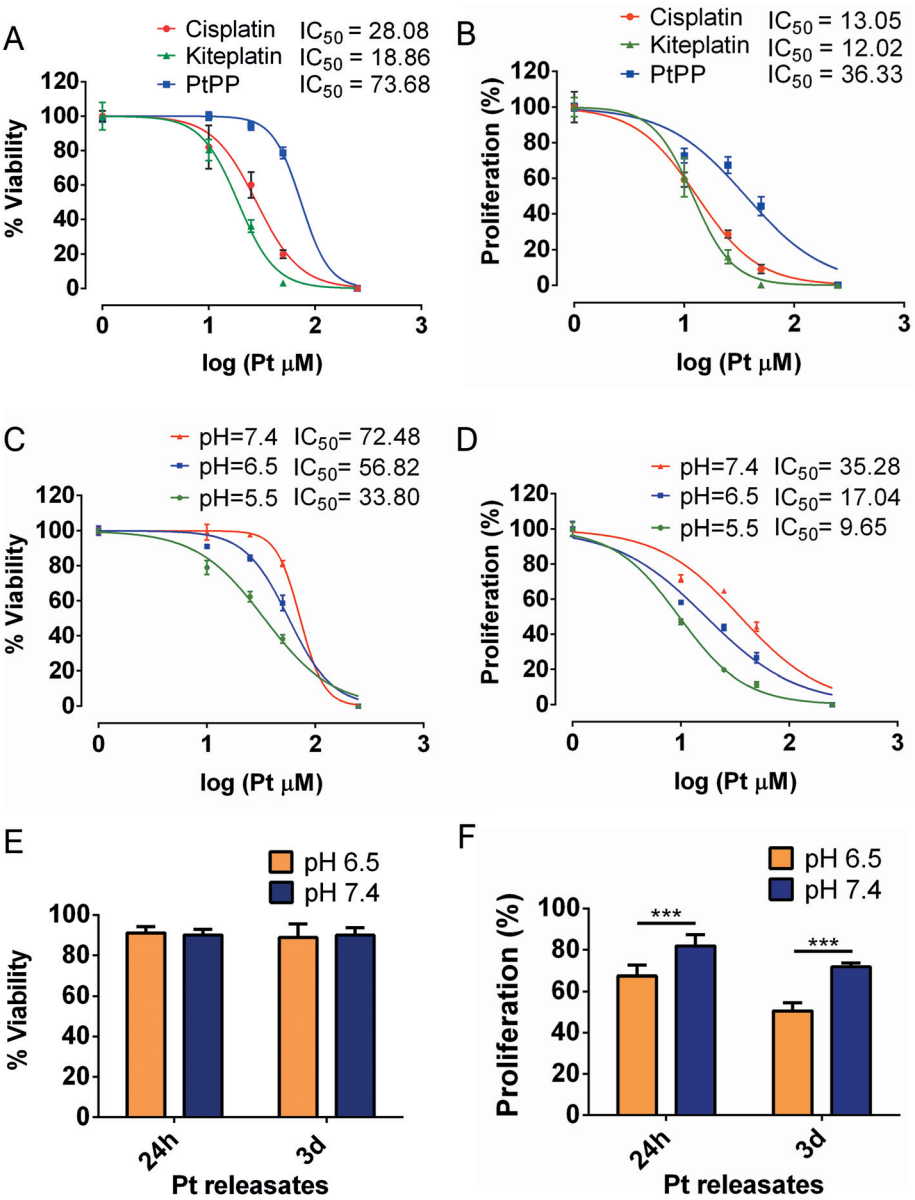

Fig. 2 *In vitro* effects of Pt compounds on human breast cancer cells. Viability (A) and proliferation (B) of breast cancer cells as a function of cisplatin, kiteplatin and PtPP concentrations. Viability (C) and proliferation (D) of breast cancer cells treated with PtPP at pH 5.5, 6.5 and 7.4 Viability (E) and proliferation (F) of breast cancer cells treated with Pt released from PtPP-loaded and citrate-functionalized HA nanoparticles. ***$P < 0.001$.

assessed at pH 6.5 and 7.4. For both assays, data were normalized against Pt-free HA nanoparticles as negative control.[40] Viability and proliferation of breast cancer cells treated with Pt-free HA nanoparticles and no treatment control are provided in Tables S4 and S5.† Pt release concentrations at both pH conditions, are shown in Table 1.

Viability of breast cancer cells remained high (~90%) irrespective of the culturing time or pH upon exposure to Pt releases (Fig. 2E). The proliferation of breast cancer cells, on the other hand, was reduced significantly by Pt species released from PtPP-loaded HA nanoparticles (Fig. 2F), especially at acidic conditions. These results clearly show that active Pt species were released under acidic conditions, thereby inhibiting cell proliferation. Summarizing, our *in vitro* cell culture and Pt quantification data evidently confirm that the cytotoxicity of Pt species released from PtPP-loaded HA nanoparticles is modulated by the local pH, which we attribute

Table 1 Pt release concentrations from PtPP-loaded HA nanoparticles

pH	Pt Concentration (μM)	
	24 h	**72 h**
7.4	14.8 ± 0.1	25.5 ± 0.1
6.5	13.3 ± 0.1	27.4 ± 0.3

to the formation of chemotherapeutically active kiteplatin species.

PtPP reduces breast cancer cell survival *in vivo*

Previously characterized embryonic zebrafish xenograft model from our group was utilized to evaluate the *in vivo* efficacy of PtPP on breast cancer cells (MDA-MB-231_eGFP).[23] Upon injection of breast cancer cells at the Duct of Cuvier, cancer cells migrated *via* the blood throughout the embryo as observed by fluorescent microscopy while few cancer cells exhibited extravasation by forming huge protrusions near the vessel wall thereby migrating towards the avascular region (Fig. S3†). For analyzing the efficacy of PtPP in the zebrafish model, first, we observed that PtPP did not induce phenotypic defects in embryos as compared to untreated embryos at Pt concentrations up to 500 μM (data not shown). *Subsequently, in vivo* experiments were carried out by (i) direct addition of PtPP into the medium surrounding embryos hosting human breast cancer cells, or (ii) by co-injecting the Pt-based drug together with breast cancer cells into zebrafish embryos. A significant reduction in the number of breast cancer cells (indicated in green in Fig. 3A) was observed 2 days after direct addition of 30 μM PtPP (29.0 ± 4.7) or co-injection of 20 μM PtPP (41.7 ± 5.5) as compared to untreated Pt-free controls (79.1 ± 5.1) (Fig. 3B). In addition, direct exposure and co-injection displayed similar therapeutic efficacy (difference between both groups was not statistically significant). Pt concentrations inside embryos hosting breast cancer cells were measured using high-resolution inductively coupled plasma-mass spectrometry (ICP-MS). These tests revealed that Pt was detected in embryos at 2 days post treatment, whereas Pt was not detected in untreated controls (Fig. S4†). Additionally, PtPP and cisplatin induced statistically similar ototoxic effects on the embryos at a concentration of 30 μm, as revealed by staining for and quantification of lateral line neuromast cells (Fig. S5A and B†). However, no neurotoxic effects were observed for both cisplatin and PtPP based on TUNEL/HuCD staining in brains (Fig. S6A and B†).

Biodistribution of fluorescently labeled HA nanoparticles in zebrafish embryos

To investigate the colloidal stability and biodistribution of citrate-functionalized (HA-Cit) nanoparticles *in vivo*, nanoparticles were tagged with a fluorescently labeled bisphosphonate AF647-zoledronate (in red) (BioVinc; Fig. S7†). Fluorescently labeled HA-Cit nanoparticles were microinjected into zebrafish embryos to monitor their biodistribution using confocal microscopy and determine potential phenotypic defects induced by these nanoparticles. As shown by Fig. 4, citrate-free HA nanoparticles (indicated in red) accumulated in *casper* embryos at the site of injection without homogeneous spreading throughout the zebrafish embryo *via* the bloodstream. On the other hand, citrate-functionalized HA nanoparticles spread throughout the embryo for concentrations ranging between 150–500 μg ml^{-1} without inducing phenotypic defects.

PtPP-loaded HA nanoparticles decreases breast cancer cell survival *in vivo*

To investigate whether PtPP-loaded HA nanoparticles released Pt to impart chemotherapeutic effects similar to direct addition of PtPP, zebrafish embryos were treated by co-injection of breast cancer cells together with freshly prepared PtPP-loaded HA nanoparticles. At 2 days post injection, embryos co-injected with eGFP-labeled breast cancer cells and PtPP-loaded HA nanoparticles showed a significant decrease in cancer cell number (30.9 ± 5.1) as compared to untreated zebrafish embryos hosting cancer cells (58.2 ± 5.2) as shown in Fig. 5A and B. These observations indicate that the zebrafish model can be used as a screening platform to verify the chemotherapeutic efficacy of drug-loaded HA nanoparticles *in vivo* in a simple and straightforward manner.

Discussion

HA nanoparticles can serve as local drug carriers *e.g.* for the prophylaxis of bone disorders such as bone metastases.[41] Prior to clinical application of drug-loaded HA nanoparticles, absorption and release of drugs from HA nanoparticles should be studied in detail using *in vivo* models. Here, we investigated – for the first time – the preclinical activity of drug-loaded HA nanoparticles to release active therapeutic species *in vivo* (similar to free drugs) against human breast cancer cells using an embryonic zebrafish xenograft model. Our study confirmed the inhibitory effects of PtPP-loaded HA nanoparticles on breast cancer cells at a very low therapeutic dose *in vivo*.

HA nanoparticles should be monodispersed and colloidally stable to facilitate reproducible local delivery *in vivo*. The colloidal stability of platelet-shaped HA nanoparticles was improved using sodium citrate. Citrate anions are effective dispersants for HA nanoparticles owing to their low toxicity, strong binding affinity for calcium ions and great dispersing efficacy.[42–45] However, citrate constitutes up to 5.5 wt% of the organic content of bone, and strongly attaches to the surface of HA. In order to exclude the influence of citrate addition on drug loading efficiency, the physicochemical properties of PtPP-loaded HA nanoparticles were studied by measuring their particle size, polydispersity index and zeta potential confirming colloidally stable nanoparticles until 8 weeks. Pt release kinetics from PtPP-loaded HA nanoparticles was dependent on pH after 72 h, whereas Ca release kinetics confirmed dissolution of HA nanoparticles at acidic pH. These results are in line with recent findings which showed that lower pH values trigger dissolution of HA nanoparticles and release of kiteplatin chemisorbed on their surface.[46]

Although conventional *in vitro* and other 3D tumor models have been used for high-throughput screening of nanoparticles and to study its effect, the complexity and dynamics involved in the *in vivo* system cannot be mimicked. In this regard, recent studies show zebrafish being used as model to understand tumor progression, metastasis and dissemination.[47] Zebrafish models mimic the biological complexity and

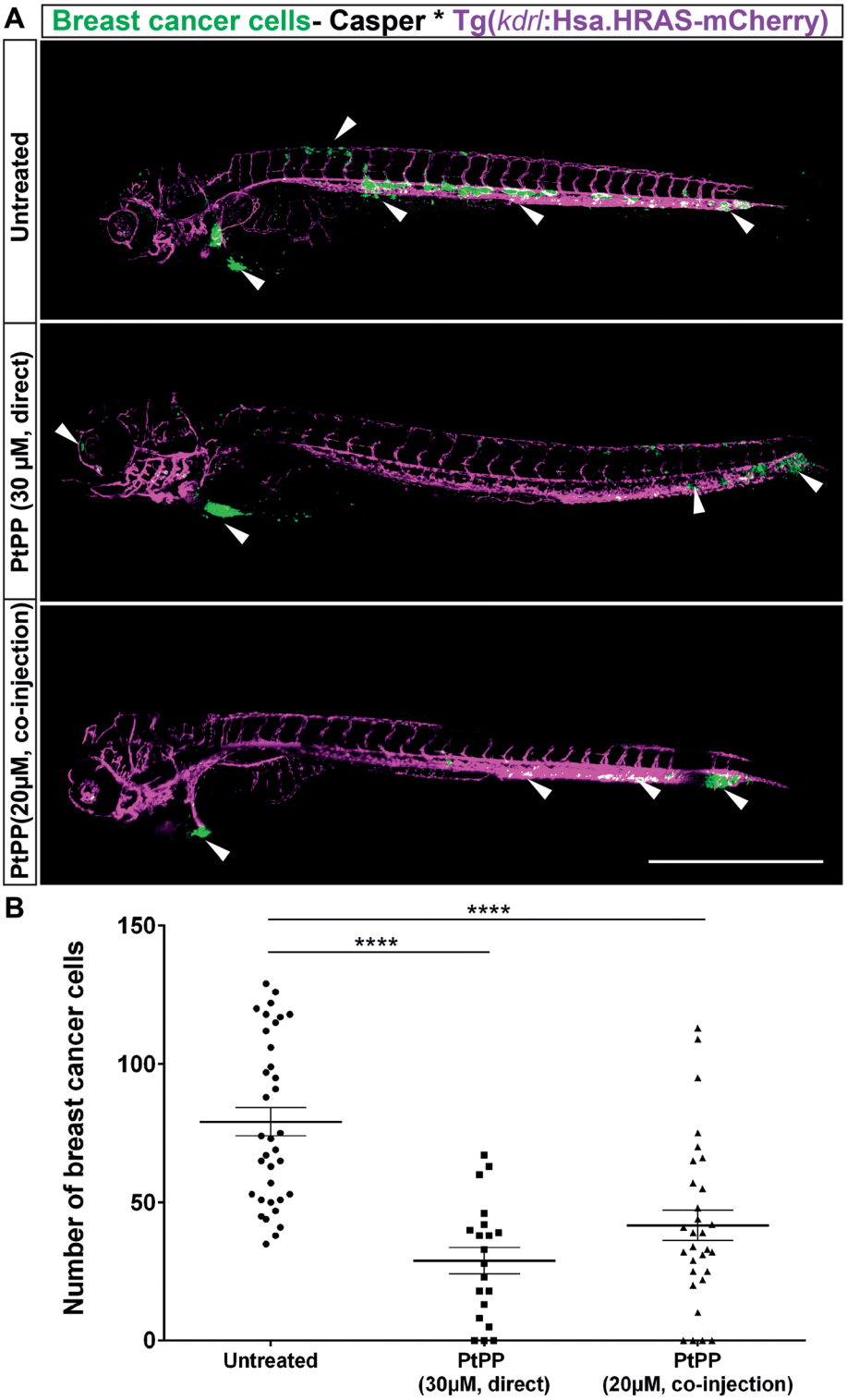

Fig. 3 Effect of direct addition or co-injection of PtPP on zebrafish embryo hosting breast cancer cells. (A) Representative images of zebrafish embryo expressing vascular marker *Tg(kdrl:Has.HRAS-mCherry)* in *casper* background hosting eGFP labeled breast cancer cells (MDA-MB-231_eGFP) at 2 days post injection: in contrast to untreated Pt-free controls, direct addition of 30 µM PtPP (center) and co-injection of 20 µM PtPP (bottom) revealed a reduction in breast cancer cell number. Vasculature is indicated in magenta and breast cancer cells are depicted in green. White arrowheads correspond to presence of cancer cells in the respective regions. Scale bar: 500 µm. (B) Manual quantification of cancer cells at 2 days post injection revealing a significant reduction of breast cancer cell number in PtPP-treated embryos compared to controls. Plot represents mean ± SEM. Statistical analysis: one-way ANOVA followed by Dunnett's test for multiple comparisons. ****$P < 0.0001$.

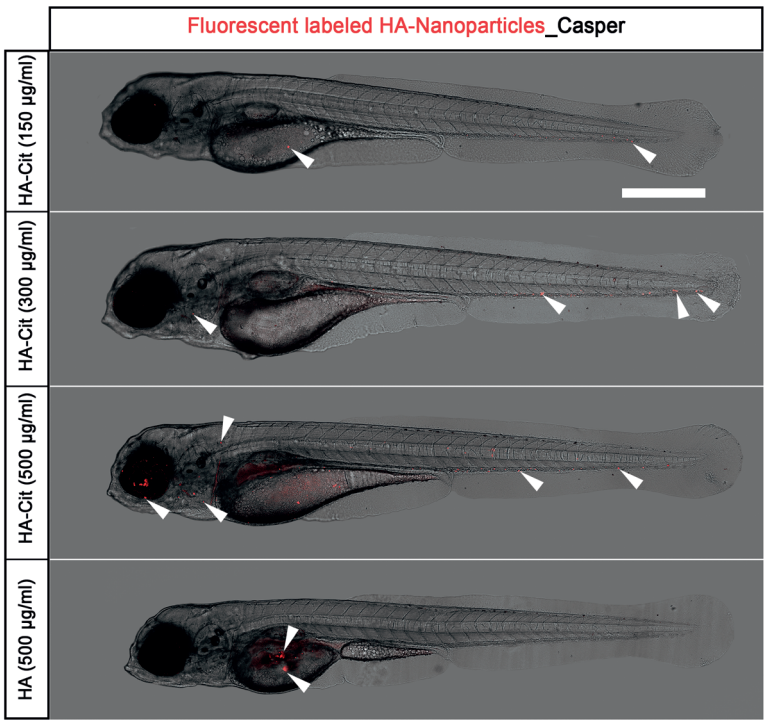

Fig. 4 Biodistribution of fluorescently labeled HA-Cit and HA nanoparticles in zebrafish embryo. Biodistribution of fluorescently labeled HA-nanoparticles (in red) injected in *casper* embryos at 2 days post injection (2 dpi). At concentrations between 150–500 µg ml^{-1}, all citrate-functionalized HA-Cit nanoparticles (top) were spread homogeneously throughout the embryos, whereas citrate-free HA nanoparticles accumulated near the injection site (bottom). HA nanoparticles are depicted in red, white arrowheads correspond to fluorescently labeled HA nanoparticles. Scale bar: 500 µm.

perfused conditions of the human tumor microenvironment more closely than simple 2D *in vitro* systems. Moreover, they allow for screening of functional cancer related-phenotypes, cell migration, extravasation and invasion properties. In addition, zebrafish models are more suitable for evaluation of local delivery of drug-loaded nanoparticles, which cannot be studied in 2D *in vitro* systems. Moreover, high-throughput screening utilizing zebrafish models as compared to mice models reduces the need for high amounts of tumor cells and drug-loaded nanoparticles by 100×.

In our previous study, we utilized high resolution selective plane illumination microscopy (SPIM) to characterize in detail, the dissemination behavior of injected human breast cancer cells *in vivo*.[23] Also, SPIM imaging allowed us to monitor the cells in real time with high spatial and temporal resolution, thereby analyzing the cancer cell behavior, migration pattern, extravasation and invasion of tumor cells into the zebrafish embryos. Also 80% of the injected cells retained inside the larvae until 3 dpi, provided sufficient window for the drug screening. Moreover, we have validated the model for anti-leukemic drug and other studies have shown a pre-treatment drug sensitivity platform for patient-derived multiple myeloma and breast tumor cells in zebrafish xenografts.[23,30,48,49]

In the current study, we have utilized the previously characterized breast metastatic zebrafish embryonic xenografts for testing the efficacy of PtPP-loaded HA nanoparticles as local drug carriers. Previous studies described that zebrafish embryos can be employed to test the toxic effects of HA nanoparticles with different shapes, albeit in an indirect manner. These studies also showed that upon indirect exposure to HA nanoparticles, the morphology and phenotype of zebrafish can be modulated, thereby delaying their development.[40,50,51] Also, aggregation of HA around the membrane protein was observed causing limited toxicity to the treated embryos.[52] However, these studies investigated nanoparticle toxicity indirectly without microinjection of HA nanoparticles into zebrafish embryos. Therefore, we microinjected HA-Cit nanoparticles into zebrafish embryos in the current study. Direct injection of colloidally stable HA nanoparticles into zebrafish embryo did not induce any phenotypic abnormalities. To our knowledge, this report shows for the first time that colloidally stable HA nanoparticles (150–500 µg ml^{-1}) can be microinjected into the blood circulation through the duct of Cuvier (DoC) of zebrafish embryo. Interestingly, the biodistribution of citrate-functionalized and fluorescently dyed HA-nanoparticles revealed a striking similarity with the distribution pattern of injected cancer cells, thereby confirming distribution of nanoparticles through the vasculature system.[23,48] Similarly, zebrafish embryos were also employed in other studies to characterize ultrabright fluorescent silica nanoparticles for targeting of xenografted human epithelial cancer cells.[53]

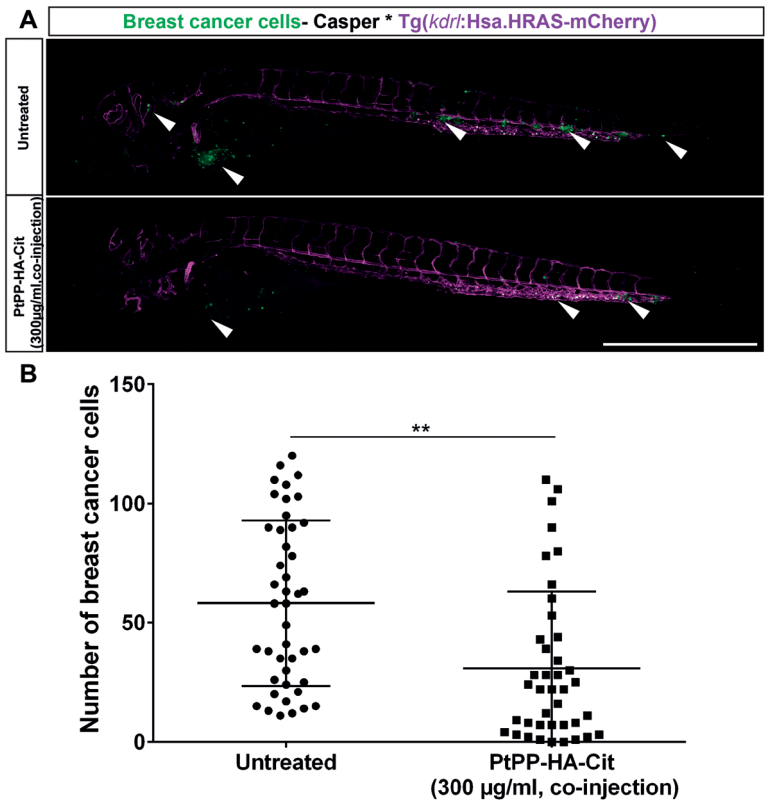

Fig. 5 Effect of PtPP-loaded and citrate-functionalized HA nanoparticles (PtPP-HA-Cit) nanoparticles on survival of breast cancer cells *in vivo*. (A) Zebrafish embryo expressing vascular marker *Tg(kdrl:Has.HRAS-mCherry)* in *casper* background injected with eGFP-labeled breast cancer cells (MDA-MB-231_eGFP) at 2 days post injection. Co-injection of 300 µg ml^{-1} of PtPP-loaded HA nanoparticles and breast cancer cells (bottom) decreased cancer cell numbers as compared to untreated controls (top). Vasculature is shown in magenta and breast cancer cells are depicted in green. White arrowheads indicate the presence of cancer cells. Scale bar: 500 µm. (B) Manual quantification of cancer cell number at 2 days post injection indicating that PtPP-loaded HA nanoparticles reduced survival of breast cancer cells in zebrafish embryos as compared to untreated controls. Plot represents mean ± SEM. Statistical analysis: two-tailed Mann Whitney U Test. $^{**}P < 0.01$.

Previously, the anti-cancer activity of PtPP has been demonstrated on a broad range of cancer cells *in vitro* comparable to oxaliplatin.[18,19] Consequently, PtPP displayed strong anti-proliferative activity against breast cancer cells at reduced pH, but the anti-proliferative activity of PtPP was substantially inferior to cisplatin and kiteplatin at neutral pH. This poor chemotherapeutic activity of PtPP under neutral conditions is attributed to the slow release of Pt from PtPP at neutral pH.[18] On the other hand, the anti-proliferative activity of PtPP increased by a factor of 4 by lowering the pH from 7.4 to 5.5. These results confirm previous *in vitro* findings indicating that PtPP readily reacts with 5′-GMP (used as a model of nucleic acids) at acidic conditions, which means that chemotherapeutically active Pt species are formed at lower pH.[18] The combined evidence of the CCK-8 and proliferation assays clearly confirmed that PtPP exhibits anti-proliferative effects on breast cancer cells particularly at reduced pH. Similarly, the Pt releasates from PtPP-loaded HA nanoparticles exhibited only anti-proliferative effect on breast cancer cells at reduced pH. This could be attributed to the lower concentration of PtPP in the Pt releasates which was not sufficient to impart a significant effect on viability of breast cancer cells. The observed results were consistent with the IC_{50} values observed for PtPP at pH 6.5 and 7.4. Moreover, the possible toxic effects of PtPP on non-cancerous cells such as bone marrow stem cells have been addressed by Barbanente *et al.*[54] Interestingly, PtPP released kiteplatin species which effectively suppressed cancer cells within a specific therapeutic window (between 11 and 28 µM), while cytotoxicity to bone marrow stem cells was reduced *in vitro*.[54]

To confirm our findings *in vivo*, we injected breast cancer cells and treated them with PtPP either directly or *via* co-injections. Two different exposure methods were employed to confirm the effect of PtPP on tumor cells *in vivo.* Additionally, this strategy revealed the minimum PtPP loading concentrations to impart similar antitumor effects. Concurrent with our *in vitro* results, our *in vivo* results confirmed that PtPP delivery led to a significant reduction in the number of breast cancer cells following both direct addition or co-injection into zebrafish. Using ICP-MS, we further affirmed that the reduction in cancer cells was due to the presence of Pt within the zebrafish embryos. However, with the direct exposure, we encountered survival issues with the injected embryos. Interestingly, direct exposure of free PtPP in zebrafish embryos

(without any injection of cancer cells) up to 500 μM did not induce any reduced survival or phenotypic abnormalities. However, survival of zebrafish embryos injected with breast cancer cells and 30 μM free PtPP treatment was considerably reduced. This may be related to indirect effects mediated by an inflammatory response reminiscent of the clinically know tumor lysis syndrome.

Similarly, co-injection of PtPP loaded, citrate functionalized HA nanoparticles effectively reduced the breast cancer cells *in vivo* compared to controls confirming effective release of Pt. The PtPP loaded HA nanoparticles were co-injected, since injection of cancer cells and nanoparticles separately (double injections) inside the embryo caused edema and reduced survival of the embryos. These *in vivo* results were compared with our *in vitro* results to validate our *in vivo* model. IC_{50} values for free PtPP ranged between 17 μM and 35 μM at pH 6.5 and pH 7.4, respectively. Interestingly, the concentration of free PtPP required to reduce tumor cell survival in zebrafish embryo (where pH varies between 6.6–8.2)[55] was found to be in the similar range of 20–30 μM, which seem to confirm the validity of the zebrafish model. Nevertheless, direct comparison between *in vitro* and *in vivo* data is not feasible for PtPP-loaded HA nanoparticles, since the concentration of Pt released *in vivo* is unknown. Still, based on the *in vitro* Pt release profile of PtPP-loaded HA nanoparticles, it can be derived that a maximum Pt concentration of 33 μM (111 μM of PtPP in 300 μg ml^{-1} of PtPP-loaded HA nanoparticles) was released after 24 h, thereby reducing cancer cells by 50%, as also observed *in vitro* at reduced pH. The *in vivo* study represents free PtPP exhibiting similar efficiency as PtPP-loaded HA nanoparticles *in vivo*. However, it should be stressed that drug-loaded HA nanoparticles allow for local instead of systemic drug delivery applications. As compared to systemic delivery of chemotherapeutic drugs, this local approach allows to increase therapeutic efficacy and reduce undesired systemic side effects.

Our study showcased the feasibility of PtPP-loaded HA nanoparticles to reduce tumor cells *in vivo* using a zebrafish model. Nevertheless, several challenges remain to be solved before clinical translation can be considered. First, detailed studies are required to provide evidence for the mechanisms of action, including investigations on nanoparticle internalization and the involvement of different host-immune compartments towards the incoming nanoparticles. More importantly, the host niche and microenvironmental cues are unknown, and thus, engrafted tumor cells are exposed to a completely different biological environment. In addition, the current model only provides insight on the short-term effect of nanoparticle-based drug formulations on tumor cell viability in a xenogenic transplant *in vivo* setting. Therefore, further investigations on the feasibility of PtPP-loaded HA nanoparticles for local treatment of bone metastases should be performed in small and large bone metastasis animal models. Nevertheless, zebrafish models offer new opportunities to study the efficacy of nanoparticles as therapeutic agents in cancer treatment.

Conclusion and outlook

Herein we evaluated the capacity of novel PtPP-loaded HA nanoparticles to reduce breast cancer cells *in vitro* and *in vivo* using a zebrafish xenograft model. Overall, we show that the embryonic zebrafish model is suitable to monitor biodistribution of colloidally stable drug-loaded HA nanoparticles and to show effective reduction of cancer cells *in vivo*. This new technology offers a versatile platform for screening of drug-loaded HA nanoparticles to facilitate subsequent validation in further preclinical models. Most importantly, we show that PtPP-loaded and citrate-functionalized HA nanoparticles effectively decrease breast cancer cells survival both *in vitro* and *in vivo* in a similar manner to free PtPP. However, the chemotherapeutic potential of PtPP-loaded HA nanoparticles for treatment of bone metastases should be studied in future *in vivo* tests using clinically relevant animal models.

Experimental section

Materials and methods

Commercial reagent-grade chemicals and solvents were used as received without further purification. Milli-Q water was used to dissolve the compounds. All other reagents were purchased from Sigma-Aldrich.

Synthesis of hydroxyapatite nanoparticles

Platelet-shaped HA nanoparticles were synthesized according to a method reported by Liou *et al.*[36] and Iafisco *et al.*[10] Briefly, apatite nanocrystals were precipitated from a suspension of Ca $(CH_3COO)_2$ (83 mM) by slow addition (1 drop s-1) of an aqueous solution of H_3PO_4 (50 mM) at a stoichiometric Ca/P ratio (1.67), keeping the pH at a constant value of 10 by the addition of a 25% $(NH_4)OH$ solution at 25 °C. The reaction mixture was stirred at room temperature for ~24 h, after which stirring was stopped and the mixture was left standing for 2 h to allow sedimentation of the nanoparticles. Subsequently, the suspension was centrifuged (2500*g* for 10 min, Eppendorf Centrifuge 5804 R, Hamburg, Germany) in Falcon 50 mL conical centrifuge tubes and washed with Milli-Q three times. Approximately half of the reaction product was suspended in Milli-Q water (39.3 mg mL) while the rest was lyophilized (no cryoprotectant applied; Freezone 4.5, Labconco, USA) for ~24 h.

Preparation and characterization of kiteplatin-pyrophosphate (PtPP)

[Pt(dihydrogen pyrophosphate)(*cis*-1,4-DACH)] was prepared as reported previously.[18] Anal. Calc. for [Pt(dihydrogenpyrophosphate)(*cis*-1,4-DACH)] ($C_6H_{16}N_2O_7P_2Pt$, M_w = 485.23 g mol^{-1}): C, 14.84%; H, 3.32%; N, 5.77%. Found: C, 14.96%; H, 3.32%; N, 5.77%. The spectroscopic characterization of the platinum complex was consistent with data reported.[18]

Stabilization of HA nanoparticles

Citrate-functionalized HA nanoparticles were prepared by treating freshly prepared 30 mg of HA nanoparticles (4.5 mL of suspension) with 89.7 mg of sodium citrate (Cit), with a final citrate concentration of 67 mM. The suspensions were stirred at room temperature for 2 h, subsequently washed twice by centrifugation (2500*g*, 5 minutes). Subsequently, the HA-Cit suspension was transferred to tubular cellulose membrane (length: 10 cm; diameter: 22 mm; cutoff: 3500 Da) and dialyzed against ultrapure water for 24 h to eliminate the unbound citrate.

Evaluation of the effect of citrate functionalization on drug adsorption

Three different adsorption procedures were explored to determine the effect of citrate adsorption on colloidal stability of HA nanoparticles and drug loading efficiency.

a. *Citrate first (CF)*: 30 mg of HA (2.07 mL of suspension) were mixed with 89.7 mg of $Na_3C_3H_5O(COO)_3$ at a final citrate concentration of 67 mM. The suspensions were stirred at room temperature for 2 h, subsequently washed twice by centrifugation (2500*g*, 5 minutes). 4.5 mg of PtPP were dissolved in 2.43 mL of water and mixed with the HA-Cit suspension. The suspension was kept under agitation at 37 °C for 24h. Thereafter, the PtPP–HA-Cit suspension was transferred to a tubular cellulose membrane (length: 10 cm; diameter: 22 mm; cutoff: 3500 Da) and dialyzed against a large excess of ultrapure water for 24 h to eliminate the unbound citrate and drug.

b. *Drug first (DF)*: 4.5 mg of PtPP were dissolved in 2.43 mL of water and mixed with 30 mg of HA (2.07 mL of suspension). The suspension was kept under agitation at 37 °C for 24h, and subsequently washed twice by centrifugation (2500*g*, 5 minutes). Afterwards, the PtPP-HA suspensions were mixed with 89.7 mg of $Na_3C_3H_5O(COO)_3$ and stirred at room temperature for 2 h. Subsequently, the PtPP- and citrate-treated HA nanoparticle suspension was transferred to a tubular cellulose membrane (length: 10 cm; diameter: 22 mm; cutoff: 3500 Da) and dialyzed against a large excess of ultrapure water for 24 h to eliminate the unbound citrate and drug.

c. *Simultaneous (S)*: 30 mg of HA (2.07 mL of suspension) were mixed with 89.7 mg of $Na_3C_3H_5O(COO)_3$. 4.5 mg of PtPP were dissolved in 2.43 mL of water and mixed with the HA suspension. The suspension was kept under agitation at 37 °C for 24 h. Subsequently, the suspension transferred to a tubular cellulose membrane (length: 10 cm; diameter: 22 mm; cutoff: 3500 Da) and dialyzed against a large excess of ultrapure water for 24 h to eliminate the unbound citrate and drug.

Finally, the nanoparticles were freeze-dried, dissolved in 2% HNO_3 aqueous solution and analyzed by ICP-OES in order to determine Ca, P ad Pt content using ICP-OES. In addition, supernatants from the various washing steps were analyzed as well using ICP-OES.

Preparation of drug-loaded HA nanoparticles

PtPP was loaded onto freshly prepared HA nanoparticles based on the drug first method as reported above. Briefly, 4.5 mg of PtPP were dissolved in 2.43 mL of water and mixed with 30 mg of HA (2.07 mL of suspension). The suspension was kept under agitation at 37 °C for 24 h, and subsequently washed twice by centrifugation (2500*g*, 5 minutes). Afterwards, the PtPP-HA suspensions were mixed with 89.7 mg of $Na_3C_3H_5O(COO)_3$ and stirred at room temperature for 2 h. Subsequently, the PtPP-loaded HA suspension was transferred to a tubular cellulose dialysis membrane (length 10 cm; diameter 22 mm; cutoff 3500 Da) and dialyzed against a large excess of ultrapure water for 24 h to eliminate the unbound citrate and drug. The total adsorption of Pt-pyrophosphate complexes onto HA nanoparticles was quantified after dissolving 1 mg of drug-loaded HA NPs in 2 wt% nitric acid. After complete dissolution of these drug-loaded NPs, the Ca and Pt concentrations were determined by ICP-OES analysis.

Drug release from HA nanoparticles

The freshly prepared drug-loaded HA nanoparticles were washed twice with Milli-Q water. 30 mg of PtPP-loaded HA nanoparticles were mixed in a glass tube with 10 mL of HEPES buffer (100 mM) at pH 7.4 or 6.5 to study the effect of pH of the release media on drug release kinetics. After 15 s of treatment in a vortex apparatus, the apatite suspension was maintained in an incubator at 37 °C shaking at 200*g*. At scheduled times, the supernatant (separated from the solid phase following 6 min of centrifugation at 2500*g*) was removed to determine Pt and Ca concentrations using ICP-MS, and replaced with fresh buffer. Cumulative Pt release was calculated relative to the total amount of Pt adsorbed onto HA nanoparticles. The values are represented as mean ± standard deviation (n = 4). The data are expressed in terms of $M/M_{tot} \times 100$, where M is the platinum complex released in ng mL^{-1} at the measured time point, and M_{tot} is the total chemisorbed complex (the initial amount of complex effectively bound to the HA-Cit).

In vitro cytotoxicity studies

PtPP was used in the *in vitro* cell culture experiments together with cisplatin as clinically used reference compound and kiteplatin. All solutions of the Pt compounds were prepared at different concentrations from a 5 mM stock solution, which was freshly prepared in Milli-Q water before use. The cytotoxic effect of the compounds was tested *in vitro* against a human breast cancer cell line (MDA-MB-231_eGFP). The cell line was maintained at 37 °C with 5% CO_2 in log phase and cultured using DMEM medium (Gibco) supplemented with 10 (v/v) % fetal bovine serum (FBS, Lonza) and 1% G418 antibiotic.

Preparation of releasates from drug-loaded hydroxyapatite nanoparticles

To assess the cytotoxic effect of Pt compounds released from PtPP-loaded HA nanoparticles, 30 mg of PtPP-loaded HA nanoparticles were incubated at acidic pH 6.5 (HEPES buffer, 100 mM) or at physiological pH 7.4 (HEPES buffer, 100 mM) to mimic the acidic tumor environment and normal physiological conditions, respectively. After 15 s of vortexing, the HA suspensions were placed in a bascule bath at 37 °C. After scheduled

time points (24 h and 72 h), the releasates were collected from the different buffer conditions by 2 minutes of centrifugation at 15 000*g*. The collected releasates (200 μL) were diluted to 2 mL of corresponding medium before the cell culture experiment. Further, the amount of Pt released from the HA nanoparticles was quantified by ICP-MS.

CCK-8 assay

The metabolic activity of MDA-MB-231_eGFP cells was quantified as a measure for cell viability using the CCK-8 assay.[56] Briefly, 5×10^3 cells per well were seeded in 96-well plates with 200 μL of growth medium. After 24 h, the medium was replaced with medium containing the Pt complex or the releasates prepared in medium as described above. After 72 h of incubation, each well was treated with 20 μl of 5 mM CCK-8 solution in 200 μl medium. The microplates were incubated at 37 °C for 2 h, after which the absorbance of each well was measured at 450 nm using a microplate reader (Bio-Tek Instruments, Inc.). 5% DMSO was used as positive control and cells not subjected to any treatment or to drug-free HA nanoparticles were used as negative control. The mean absorbance for each group was plotted based on the percentage of absorbance of the negative control. The values are represented as mean ± standard deviation (n = 4). For CCK-8 assay, cancer cell viability was plotted over a range of concentrations to compare the inhibitory concentration (IC_{50}) of PtPP with kiteplatin and cisplatin (as commonly used Pt drugs). Data are represented by mean ± standard deviation (n = 4).

Proliferation assay

DNA content was quantified as a measure for cell proliferation using the Quant-iT Picogreen dsDNA Kit (Invitrogen) according to the instructions of the manufacturer. A DNA standard curve was used to quantify the amount of DNA in each well and the results were measured using a fluorescence microplate reader (Bio-Tek Instruments Inc.) with an excitation wavelength at 485 nm and an emission wavelength at 530 nm. A standard curve was prepared in duplicate for each 96-well plate. The PicoGreen (PG) dsDNA quantitation reagent was diluted on the day of the experiment by making a 200-fold dilution in 1× Tris-EDTA working solution. This PG working solution was prepared with protection from light, as suggested by the manufacturer. After performing CCK-8 assays, cells were prepared by washing the cell layers twice with PBS and adding 200 μl Milli-Q water to each well, after which repetitive freezing (−20 °C) and thawing (37 °C) cycles were performed. Subsequently, 100 μl of either sample or standard was added to the wells, followed by 100 μl of 1× PG solution. The plates were incubated in the dark for 5 min at room temperature. Following incubation, plates were read on a fluorescent microplate reader (Bio-Tek Instruments, Inc.) with excitation and emission settings of 485 and 538 nm, respectively. Results were fitted to the DNA standard curve to determine DNA concentrations of the cells. To determine the percentage of proliferation capacity of different treatment groups, the DNA concentration were normalized to the negative controls. Data are represented by mean ± standard deviation (n = 4).

In vivo studies

Animal care and handling: All animal procedures were performed in accordance with the Guidelines for Care and Use of Laboratory Animals of the Federal Republic of Germany (Tierschutzgesetz), approved by the Landesdirektion Sachsen (DD24-5131/346/11 and DD24-5131/346/12) in accordance with EU directive 2010/63/EU. The Casper strain of Danio rerio zebrafish were maintained under standard conditions (28 °C in E3 buffer) until 48 hours post fertilization (hpf) as described previously.[57] All animal experiments were conducted at larval stages before the point of independent feeding and were in agreement with the animal protection law (Tierschutzgesetz). Cancer cells (MDA-MB-231_eGFP) were loaded in a glass capillary and microinjected into the blood circulation *via* the duct of Cuvier (DoC) of zebrafish lines (Casper[58] and Tg(kdrl:Has. HRAS-mCherry))[59] as described previously.[23] Engrafted embryos were maintained in a new Petri dish at 33 °C. Based on the spreading of fluorescently labeled breast cancer cells in the embryos at 2 hours post injection, embryos with breast cancer cells in the blood circulation were selected for further experiments.

Image acquisition and processing

For quantification, embryos were fixed in 4% paraformaldehyde at 4 °C overnight. Fixed embryos were imaged using inverted confocal microscopy (Zeiss LSM 780) at 20x magnification (whole embryos). Confocal stacks were converted to maximum intensity projections using Image J (v 1.51h) for representative images. The quantification of cancer cell survival at 2 dpi was performed manually with confocal microscopy by going through individual stacks.

Drug treatment and efficiency evaluation

The *in vivo* experiments were designed to initially confirm the *in vitro* results on the antitumor efficacy of free PtPP using a zebrafish model. This was crucial to confirm the antitumor efficacy of free PtPP *in vivo* for first time. In addition, this experimental design also enabled us to determine the minimum concentration of PtPP required to induce antitumor effects *in vivo*. PtPP concentrations were selected based on a preceding pilot study in zebrafish embryos (data not published). Preliminary results indicated a dose-dependent effect: direct addition required a minimum of 30 μM free PtPP concentration to reduce the tumor cells whereas 20 μM of free PtPP was sufficient to reduce the tumor cells when co-injected. Unless specified otherwise, all stocks and working solutions were prepared in water. For PtPP, a working concentration of 30 μM was prepared from 1 mM stock and added to E3 medium containing embryos. For co-injections with cancer cells, a 20 μM solution was used and injection volume of ~3–4 nl was used. For PtPP-loaded HA nanoparticles, a nanoparticle concentration of 300 μg ml^{-1} was prepared from a 1 mg ml^{-1} stock. Based on ICP-MS, the PtPP concentration was measured

as 370 μM for this 1 mg ml^{-1} stock of PtPP-loaded HA nanoparticles. Cancer cell survival after each drug treatment, from days 1–2 post-treatment, was assessed by fluorescence microscopy and cell numbers were quantified manually.

Statistical analyses

All *in vitro* results are represented as mean ± standard deviation and *in vivo* results are represented as mean ± sem. Statistical analyses were performed using GraphPad Prism (version 6.04) software. Differences among groups in the adsorption and release studies were determined by two-way analysis of variance (ANOVA) with *post hoc* Bonferroni (multiple comparisons) test. The statistical analysis of the CCK-8 assay and proliferation assay was performed by means of a two-way ANOVA with a Dunnett (multiple comparisons) *post hoc* test with cisplatin or hydroxyapatite treatment as control. For all *in vivo* experiments, unless indicated otherwise, two-tailed Mann–Whitney U test or one-way Analysis of Variance (ANOVA) was performed followed by Dunnett's *post-hoc* method for multiple comparisons. For all statistical analyses, a value of p was considered as significantly different if $*P < 0.05$; $**P < 0.01$; $***P < 0.001$; $****P < 0.0001$.

Authors contributions

R.A.N. and N.A. contributed equally to this work. R.A.N., N.A., M.I., N.M., M.Bo., J.J.J.P.B., and S.C.G.L designed the research. A.C., and N.M provided the materials. R.A.N., L.D.E., and A.C synthesized and characterized nanoparticles. R.A.N and A.B performed *in vitro* experiments. A.C., A.B., and N.M performed NMR experiment. R.A.N., L.S., and U.K performed the ICP-MS measurements. N.A performed the zebrafish experiment and analyzed data. R.A.N., N.A., M.I., N.M., M.Br., M.Bo., and S.C.G.L analyzed data. R.A.N., N.A., J.J.J.P.B., M.Bo., and S.C.G.L. wrote the manuscript. All authors read and corrected the manuscript.

Conflicts of interest

There are no conflicts to declare.

Acknowledgements

The authors thank Dr. Stefan Hans for support with the zebrafish ototoxicity assay. The table of contents figure was created with Biorender. The authors are grateful for the funding support from the Radboud Institute for Molecular Life Science (RIMLS grant #014-057), Radboud University Medical Center.

References

1 S. Bose and S. Tarafder, *Acta Biomater.*, 2012, **8**, 1401–1421.
2 H. Cheng, A. Chawla, Y. Yang, Y. Li, J. Zhang, H. L. Jang and A. Khademhosseini, *Drug Discovery Today*, 2017, **22**, 1336–1350.
3 S. Mondal, S. V. Dorozhkin and U. Pal, *Wiley Interdiscip. Rev.: Nanomed. Nanobiotechnol.*, 2018, **10**, e1504.
4 V. S. Kattimani, S. Kondaka and K. P. Lingamaneni, *Bone Tissue Regen. Insights*, 2016, **7**, BTRI.S36138.
5 C. Rey, C. Combes, C. Drouet, S. Cazalbou, D. Grossin, F. Brouillet and S. Sarda, *Prog. Cryst. Growth Charact. Mater.*, 2014, **60**, 63–73.
6 T. Boix, J. Gomez-Morales, J. Torrent-Burgues, A. Monfort, P. Puigdomenech and R. Rodriguez-Clemente, *J. Inorg. Biochem.*, 2005, **99**, 1043–1050.
7 J. Jeong, J. H. Kim, J. H. Shim, N. S. Hwang and C. Y. Heo, *Biomater. Res.*, 2019, **23**, 4.
8 N. C. Daw, C. A. Billups, C. Rodriguez-Galindo, M. B. McCarville, B. N. Rao, A. M. Cain, J. J. Jenkins, M. D. Neel and W. H. Meyer, *Cancer*, 2006, **106**, 403–412.
9 R. Sciuto, A. Festa, S. Rea, R. Pasqualoni, S. Bergomi, G. Petrilli and C. L. Maini, *J. Nucl. Med.*, 2002, **43**, 79–86.
10 B. Palazzo, M. Iafisco, M. Laforgia, N. Margiotta, G. Natile, C. L. Bianchi, D. Walsh, S. Mann and N. Roveri, *Adv. Funct. Mater.*, 2007, **17**, 2180–2188.
11 M. Iafisco, B. Palazzo, M. Marchetti, N. Margiotta, R. Ostuni, G. Natile, M. Morpurgo, V. Gandin, C. Marzano and N. Roveri, *J. Mater. Chem.*, 2009, **19**, 8385–8392.
12 M. Iafisco and N. Margiotta, *J. Inorg. Biochem.*, 2012, **117**, 237–247.
13 M. Iafisco, B. Palazzo, G. Martra, N. Margiotta, S. Piccinonna, G. Natile, V. Gandin, C. Marzano and N. Roveri, *Nanoscale*, 2012, **4**, 206–217.
14 M. Benedetti, F. De Castro, A. Romano, D. Migoni, B. Piccinni, T. Verri, M. Lelli, N. Roveri and F. P. Fanizzi, *J. Inorg. Biochem.*, 2016, **157**, 73–79.
15 K. Farbod, K. Sariibrahimoglu, A. Curci, A. Hayrapetyan, J. N. Hakvoort, J. J. van den Beucken, M. Iafisco, N. Margiotta and S. C. Leeuwenburgh, *Tissue Eng., Part A*, 2016, **22**, 788–800.
16 N. Margiotta, C. Marzano, V. Gandin, D. Osella, M. Ravera, E. Gabano, J. A. Platts, E. Petruzzella, J. D. Hoeschele and G. Natile, *J. Med. Chem.*, 2012, **55**, 7182–7192.
17 V. Brabec, J. Malina, N. Margiotta, G. Natile and J. Kasparkova, *Chemistry*, 2012, **18**, 15439–15448.
18 A. Curci, V. Gandin, C. Marzano, J. D. Hoeschele, G. Natile and N. Margiotta, *Inorg. Chem.*, 2017, **56**, 7482–7493.
19 J. Kasparkova, H. Kostrhunova, V. Novohradsky, J. Pracharova, A. Curci, N. Margiotta, G. Natile and V. Brabec, *Dalton Trans.*, 2017, **46**, 14139–14148.
20 C. Khanna and K. Hunter, *Carcinogenesis*, 2005, **26**, 513–523.
21 Y. Kang, in *Cancer Stem Cells. Methods in Molecular Biology (Methods and protocls)*, ed. J. S. Yu, Humana Press, 2009, vol. 568.
22 J. F. Amatruda and E. E. Patton, in *International Review of Cell and Molecular Biology*, Academic Press, 2008, vol. 271, pp. 1–34.

23 N. Asokan, S. Daetwyler, S. Bernas, C. Schmied, S. Vogler, K. Lambert, M. Wobus, M. Wermke, G. Kempermann, J. Huisken, M. Brand and M. Bornhäuser, *bioRxiv*, 2017, 215921, DOI: 10.1101/215921.
24 K. Stoletov and R. Klemke, *Oncogene*, 2008, **27**, 4509–4520.
25 L. I. Zon and R. T. Peterson, *Nat. Rev. Drug Discovery*, 2005, **4**, 35–44.
26 T. E. North, W. Goessling, C. R. Walkley, C. Lengerke, K. R. Kopani, A. M. Lord, G. J. Weber, T. V. Bowman, I. H. Jang, T. Grosser, G. A. Fitzgerald, G. Q. Daley, S. H. Orkin and L. I. Zon, *Nature*, 2007, **447**, 1007–1011.
27 M. Konantz, T. B. Balci, U. F. Hartwig, G. Dellaire, M. C. Andre, J. N. Berman and C. Lengerke, *Ann. N. Y. Acad. Sci.*, 2012, **1266**, 124–137.
28 P. Letrado, I. de Miguel, I. Lamberto, R. Diez-Martinez and J. Oyarzabal, *Cancer Res.*, 2018, **78**, 6048–6058.
29 W. Goessling, T. E. North and L. I. Zon, *J. Clin. Oncol.*, 2007, **25**, 2473–2479.
30 J. Lin, W. Zhang, J. J. Zhao, A. H. Kwart, C. Yang, D. Ma, X. Ren, Y. T. Tai, K. C. Anderson, R. I. Handin and N. C. Munshi, *Blood*, 2016, **128**, 249–252.
31 M. Haldi, C. Ton, W. L. Seng and P. McGrath, *Angiogenesis*, 2006, **9**, 139–151.
32 M. van Pomeren, N. R. Brun, W. Peijnenburg and M. G. Vijver, *Aquat. Toxicol.*, 2017, **190**, 40–45.
33 X. Zhang, J. Song, A. Klymov, Y. Zhang, L. de Boer, J. A. Jansen, J. J. van den Beucken, F. Yang, S. A. Zaat and S. C. Leeuwenburgh, *Int. J. Nanomedicine*, 2018, **13**, 5377–5394.
34 E. Haque and A. C. Ward, *Nanomaterials*, 2018, **8**, 561.
35 S. C. Leeuwenburgh, I. D. Ana and J. A. Jansen, *Acta Biomater.*, 2010, **6**, 836–844.
36 S.-C. Liou, S.-Y. Chen, H.-Y. Lee and J.-S. Bow, *Biomaterials*, 2004, **25**, 189–196.
37 S. K. Parks, J. Chiche and J. Pouyssegur, *Nat. Rev. Cancer*, 2013, **13**, 611–623.
38 D. Neri and C. T. Supuran, *Nat. Rev. Drug Discovery*, 2011, **10**, 767–777.
39 A. Dhawan, M. von Bonin, L. J. Bray, U. Freudenberg, E. Pishali Bejestani, C. Werner, L. C. Hofbauer, M. Wobus and M. Bornhauser, *Stem Cells*, 2016, **34**, 2224–2235.
40 J. Xu, P. Xu, Z. Li, J. Huang and Z. Yang, *J. Biomed. Mater. Res., Part A*, 2012, **100**, 738–745.
41 S. Mondal and U. Pal, *J. Drug Deliv. Sci. Technol.*, 2019, **53**, 101131.
42 J. M. Delgado-López, R. Frison, A. Cervellino, J. Gómez-Morales, A. Guagliardi and N. Masciocchi, *Adv. Funct. Mater.*, 2014, **24**, 1090–1099.
43 J. M. Delgado-Lopez, M. Iafisco, I. Rodriguez, A. Tampieri, M. Prat and J. Gomez-Morales, *Acta Biomater.*, 2012, **8**, 3491–3499.
44 C. Zhang, C. Li, S. Huang, Z. Hou, Z. Cheng, P. Yang, C. Peng and J. Lin, *Biomaterials*, 2010, **31**, 3374–3383.
45 Y. Y. Hu, A. Rawal and K. Schmidt-Rohr, *Proc. Natl. Acad. Sci. U. S. A.*, 2010, **107**, 22425–22429.
46 M. Lelli, N. Roveri, C. Marzano, J. D. Hoeschele, A. Curci, N. Margiotta, V. Gandin and G. Natile, *Dalton Trans.*, 2016, **45**, 13187–13195.
47 K. R. Astell and D. Sieger, *Cold Spring Harbor Perspectives in Medicine*, 2019, DOI: 10.1101/cshperspect.a037077.
48 C. Tulotta, C. Stefanescu, E. Beletkaia, J. Bussmann, K. Tarbashevich, T. Schmidt and B. E. Snaar-Jagalska, *Dis. Model. Mech.*, 2016, **9**, 141–153.
49 Y. Drabsch, S. He, L. Zhang, B. E. Snaar-Jagalska and P. ten Dijke, *Breast Cancer Res.*, 2013, **15**, R106.
50 S. Pujari-Palmer, X. Lu and M. Karlsson Ott, *Nanomaterials*, 2017, **7**, 89.
51 X. Zhao, K. J. Ong, J. D. Ede, J. L. Stafford, K. W. Ng, G. G. Goss and S. C. Loo, *Small*, 2013, **9**, 1734–1741.
52 Z. Xu, Y. L. Zhang, C. Song, L. L. Wu and H. W. Gao, *PLoS One*, 2012, **7**, e32818.
53 S. Peerzade, X. Qin, F. J. F. Laroche, S. Palantavida, M. Dokukin, B. Peng, H. Feng and I. Sokolov, *Nanoscale*, 2019, **11**, 22316–22327.
54 A. Barbanente, R. A. Nadar, L. D. Esposti, B. Palazzo, M. Iafisco, J. J. J. P. van den Beucken, S. C. G. Leeuwenburgh and N. Margiotta, *J. Mater. Chem. B*, 2020, **8**, 2792–2804.
55 R. W. Kwong, Y. Kumai and S. F. Perry, *J. Exp. Biol.*, 2014, **217**, 651–662.
56 H. Tominaga, M. Ishiyama, F. Ohseto, K. Sasamoto, T. Hamamoto, K. Suzuki and M. Watanabe, *Anal. Commun.*, 1999, **36**, 47–50.
57 M. Brand, M. Granato and C. Nuesslein-Volhard, *Keeping and raising zebrafish. In Zebrafish: A Practical Approach*, Oxford University Press, 2002.
58 R. M. White, A. Sessa, C. Burke, T. Bowman, J. LeBlanc, C. Ceol, C. Bourque, M. Dovey, W. Goessling, C. E. Burns and L. I. Zon, *Cell Stem Cell*, 2008, **2**, 183–189.
59 N. C. Chi, R. M. Shaw, S. De Val, G. Kang, L. Y. Jan, B. L. Black and D. Y. Stainier, *Genes Dev.*, 2008, **22**, 734–739.